



Investigation of Vibration Control Performance with Modified Motion Planning Based on Basic Functions for Composite Robot Manipulators

M. Uyar¹

Received: 4 July 2022 / Accepted: 28 March 2023 / Published online: 26 May 2023
© The Author(s), under exclusive licence to Shiraz University 2023

Abstract

When flexible manipulators complete their movements to the desired position, vibrations occur at the endpoint. Reducing vibrations is an important advantage for eliminating positioning errors and monitoring position accuracy. However, the increase in vibration amplitudes leads to the inability to complete the planned tasks in the applications and results in loss of productivity. Therefore, the reduction of end-effector vibrations is an important research area. In this study, a motion-based control (MBC) method with designed motion profiles is introduced to reduce the endpoint vibrations of epoxy–glass-reinforced composite manipulators. Three different motion profiles, namely Modification-1, Modification-2, and Modification-3, are designed according to time and maximum velocity values depending on the system's frequencies. For the design of Modification-1, variable deceleration and acceleration times are considered, while for Modification-2 and Modification-3, both the maximum angular velocity and the deceleration and acceleration times are utilized. For two different angular positions and motion times, all motion profiles are applied to two composite manipulators with different frequencies, and the results are experimentally and numerically obtained to examine the vibration performance of MBC. Simulation results confirmed with experiments are achieved using mathematical models in ANSYS. To evaluate the effectiveness of MBC, the change in RMS values of endpoint vibration responses and the reduction rates are presented comparatively for all motion profiles. The results show significant advantages for the MBC method, reducing vibrations by approximately 99%, and eliminating positioning errors caused by vibrations.

Keywords Composite manipulator · Endpoint vibrations · Motion-based control · Modified motion planning

List of Symbols

MBC	Motion-based control	$[M]$	Mass matrix
FCM	Flexible composite manipulator	$[K]$	Stiffness matrix
RMS	Root mean square	$[C]$	Damping matrix
FFT	Fast Fourier transform	WBS	Wireless acceleration base station
FE	Finite element	WS	Wireless acceleration sensor
FBM	Flexible body motion	O/I	Outputs/inputs
RBM	Rigid body motion	NI	National Instruments
RAS	Residual acceleration signal	t_a	Acceleration time (s)
L	Length (mm)	t_c	Constant time (s)
h	Height (mm)	t_d	Deceleration time (s)
b	Thickness (mm)	t_m	Motion time (s)
L_s	Distance of sensor point from endpoint (mm)	t_r	Residual time (s)
α and β	Rayleigh damping coefficients	t_s	Settling time (s)
K_m	Motor rotational spring constant (Nm/rad)	ω_{\max}	Maximum angular velocity (rad/s)
		$\omega(t)$	Angular velocity profile
		θ_m	Stopping angular position, degrees or radians
		dt	The step time (s)
		f_1	First natural frequency (Hz)
		t_n	Time parameter of motion profiles (s)

✉ M. Uyar
muyar@bayburt.edu.tr

¹ Department of Mechanical Engineering, Bayburt University, 69000 Bayburt, Turkey

w_d	Frequency parameter of Modification-1 and Modification-3 motion profiles
ζ	Variable of Modification-1 and Modification-3 motion profiles, $\zeta = 0.1, 0.2, \dots, 0.9$
r_z	Deceleration time variable of Modification-1 and Modification-3 motion profiles, $r_z = 1, 2, 3$
r_c	Trapezoidal and triangular profile parameter, $r_c = 0, 2$
r_n	Variable of Modification-2 motion profile, $r_n = 0, 0.5, 1, 1.5, \dots$
t_{1m}	Variable depending on the decreased time

1 Introduction

With the advances in the manufacturing industry, robot arms are replacing manpower in order to increase production, reduce costs, and improve safety. Vibrations at the endpoints of the robot arms during the execution of their planned tasks cause planning errors and problems in trajectory tracking (Alandoli et al. 2016; Kiang et al. 2015). For this reason, rigid manipulators are used to ensure the accuracy of the endpoints. However, rigid manipulators cause a decrease in the power/efficiency ratio due to high weight and energy consumption. Because of the disadvantages of rigid manipulators, the use of flexible manipulators is preferred due to their low energy consumption requirement, much lighter weight and lower cost (Alandoli et al. 2016; Faris et al. 2009; Lochan et al. 2016; Sayahkarajy et al. 2016). Flexible manipulators offer advantages in a variety of industrial applications such as space exploration (Aikenhead et al. 1983), nuclear medicine cancer therapy applications (Meggiolaro et al. 2004), and especially material handling, palletizing, automated assembly, drilling, and welding in industrial applications (Moghaddam and Nof 2016), with low torque requirements and energy consumption due to their flexibility and light weight. However, because of the light weight of flexible manipulators, vibrations are inevitable, especially when performing high-speed tasks (Rahimi and Nazemizadeh 2014). Therefore, the decreased work sensitivity and payload carrying capacity of flexible manipulators due to endpoint vibrations will cause an increase in cycle time during pick-and-place applications (Ghariblu and Korayem 2006; Korayem et al. 2011). Researchers have investigated different control applications in the literature (Alandoli and Lee 2020; Benosman and Le Vey 2004; Kiang et al. 2015; Sayahkarajy et al. 2016) on reducing endpoint vibrations of flexible manipulators, increasing task precision and efficiency, and achieving precise positioning accuracy in high-speed operations.

Motion control methods are widely used in applications such as automation machines, machine tools and manipulators. Motion control is a passive vibration control method

that does not require an additional actuator. However, active control approaches utilized with an additional actuator and system (Preumont 2018) and hybrid control applications where passive and active control methods are used together are more effective for damping vibrations. Since the use of an extra actuator in active control applications has a serious economic cost to the user, the availability of a motion control method that will eliminate the disadvantages of passive control compared to active control will be an important factor in the preference for flexible manipulators in applications. In this study, a new motion-based vibration control is proposed that consists of motion profiles with three different modifications, and their performance in controlling the vibration responses of a single-link flexible manipulator made of composite material is examined comparatively.

Because of the flexibility inherent in flexible manipulators, there is a need to create a mathematical model that will accurately represent the dynamic behavior of the system. In particular, the correct modeling of dynamic behavior is an important factor in the validation of experimental studies. In previous studies, the finite element method (FEM) (Esfandiari and Korayem 2015; Malgaca and Uyar 2019; Uyar 2022), assumed mode method (AMM) (Benosman and Le Vey 2004; Rezaei and Shafei 2019), and lumped parameter model (LPM) (Kim 2015; Tinkir et al. 2010) have been widely used to create a correct mathematical model of a flexible manipulator. With advances in materials science, approaches such as ANSYS-based FEM and system identification are used to produce flexible manipulators from various composite materials and to model their dynamic behavior (Malgaca et al. 2020; Malgaca and Lök 2021; Shitole and Sumathi 2015; Wang and Lou 2019). ANSYS also allows the geometric features of the system to be accurately represented with the FE modeling method. In conclusion, FEM offers great possibilities for validating experimental results. In our study, the ANSYS-based FE modeling method is chosen to create dynamic models of composite manipulators, due to both its ease of modeling and its ability for rapid calculation.

From the point of view of flexible manipulators, the trajectory of motion must be well planned in order to reduce endpoint vibrations in high-speed pick-and-place tasks to increase efficiency and achieve faster cycle times (Li et al. 2009; Pellicciari et al. 2013). Two different trajectory planning methods, coordinate-based and path-based (Gauthier et al. 2006), have been studied. Compared to path-based trajectory planning, trajectory planning defined with a revolute joint is easier to perform. It is realized by creating motion profiles for the revolute joint according to the design requirements (Liu et al. 2013). Suppressing the vibrations of flexible manipulators along the trajectory and at the endpoint in high-speed operations is an important problem. In view of this, velocity profiles consisting of more complex polynomial equations were developed to realize smoother

movement (Wu and Sun 2019). Machmudah et al. (2013) examined the performance of genetic algorithm (GA) and particle swarm optimization (PSO) methods to minimize the travel time, maximum torque, and acceleration of a sixth-order polynomial motion curve during the movement of a three-degree-of-freedom (3-DOF) planar robot from one position to another, taking into account complex geometric obstacles. Boryga and Grabos (2009) presented the displacement, acceleration and vibration responses of an end effector using 5-, 7- and 9-degree polynomial acceleration profiles to plan the trajectory motion of a 3-DOF serial-link manipulator. High-order polynomial motion profiles tend to deteriorate numerically as the high oscillation characteristic and polynomial order increase, in addition to creating a significant computational load in the evaluation of the polynomial coefficients. Motion profiles from lower-order polynomials, spline, trapezoidal (Macfarlane and Croft 2003; Uyar 2022) and s-curve (Malgaca and Lök 2021; Nguyen et al. 2008) functions can be used to overcome undesirable situations arising from the motion profile. For example, they are preferred by some researchers (Abu-Dakka et al. 2017; Saravanan and Ramabalan 2008) because of their use in preventing significant vibrations with motion profiles produced by the cubic spline function. Kucuk (2017) developed an optimal trajectory generation algorithm (OTGA), which consists of cubic splines that create less overshoot and vibration, in order to achieve accurate trajectory tracking with minimum movement times of serial and parallel manipulators. Perumaal and Jawahar (2012) considered the acceleration, constant, and deceleration times of the trigonometric s-curve motion profiles to develop the trajectory of a 6-DOF robotic manipulator with minimal execution time and fewer vibration values. Flexible manipulators require an active numerical solver that includes time-consuming processes for the analysis of motion profiles designed with optimization methods in industrial applications (Fang et al. 2020). However, it is preferred to use motion curves consisting of simple algorithms for real-time application in robot arms. Moreover, a robust controller, which is a combination of input shaping and closed-loop feedback linearization, has been proposed to reduce the vibrations at the end of the flexible robot arm and eliminate the error (Efafi et al. 2022).

The abovementioned studies on vibration control and trajectory tracking based on motion profiles indicate their wide use in vibration control of motion profiles produced from trapezoidal, s-curve and high-order polynomials. In this study, trapezoidal motion profiles are proposed with three different modifications that significantly reduce the endpoint vibrations of composite manipulators. The proposed motion profiles are investigated both by changing the method used to determine the parameters in the deceleration time and by the effect of the change of the parameters in the acceleration and constant times on the vibration response. Compared to

existing trapezoidal-based motion profiles, the newly modified motion profiles have distinctive features. Motion profiles provide significant ease of application because they do not require complex algorithms. In this work, motion profiles that provide motion-based vibration control are developed for industrial applications, where time and angular velocity parameters can be obtained with easy mathematical formulae without relying on complex algorithms designed with kinematic constraints. The design also provides trajectory planning that can be easily applied analytically to flexible manipulators. Moreover, it allows us to scan in more precise time steps to examine the effect of each time parameter of the trapezoidal motion profile on motion control. Using the proposed motion profiles, motion-based control to reduce vibrations can be quickly and precisely synchronized for application to general-purpose serial and parallel robotic manipulators, high-degree-of-freedom robots and computer numerical control (CNC) machines.

2 Dynamic Finite Modeling

In this work, studies are performed on a single-link flexible composite manipulator (FCM). The composite manipulator consists of a composite link produced from an epoxy–glass composite material with the orientation $[0/90/0/0/90/0]$ and six layers. The general coordinate axis is defined at the A point and the revolute joint is determined at the same point. The FCM rotates around the z-axis at the A point. In order to measure the endpoint vibrations of the FCM, the acceleration sensor with the payload effect is fixed at the tip point (sensor point). Dynamic transient analysis is performed using ANSYS. The finite element (FE) model utilizing material and geometric properties with the dynamic modeling criteria is created in three dimensions. The schematic view and dynamic FE model with lay-up configuration considered in this paper is shown in Fig. 1.

In the FE model, the composite link is represented by a Solid186 layered solid element, and the weight of the sensor as the payload is defined by a Mass21 element. The Solid186 layered element is a higher-order three-dimensional element and displays quadratic displacement behavior. Solid186, which is characterized by 20-node translations in the nodal x, y, and z directions per node, supports large strain capabilities, large deflection, and stress stiffening. In order to model the layered solids with Solid186, the element setting is adjusted as a layered option (KEYOPT(3),1). The Mass21 element, which has six degrees of freedom with the nodal x, y, and z translation directions and their rotational axes, is a point element in which a different mass and rotary inertia are assigned for each coordinate direction. The geometric properties of Solid186 and Mass21 elements are shown in Fig. 2.

Fig. 1 a Schematic view and b dynamic model of the composite manipulator

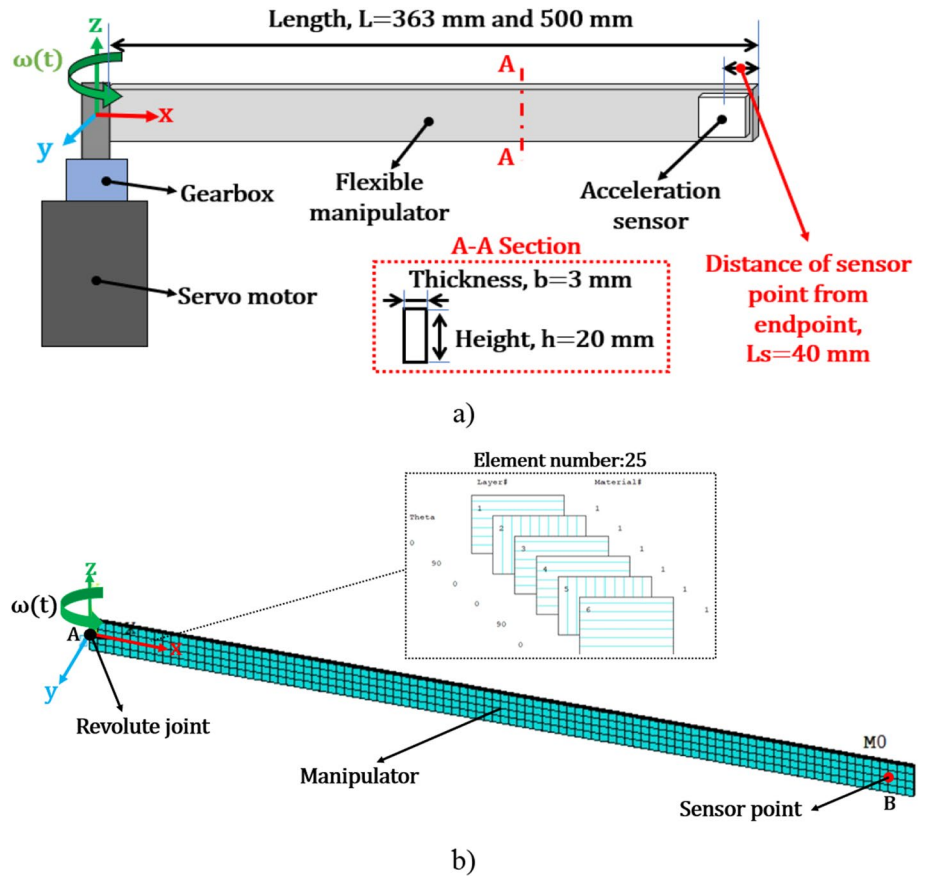
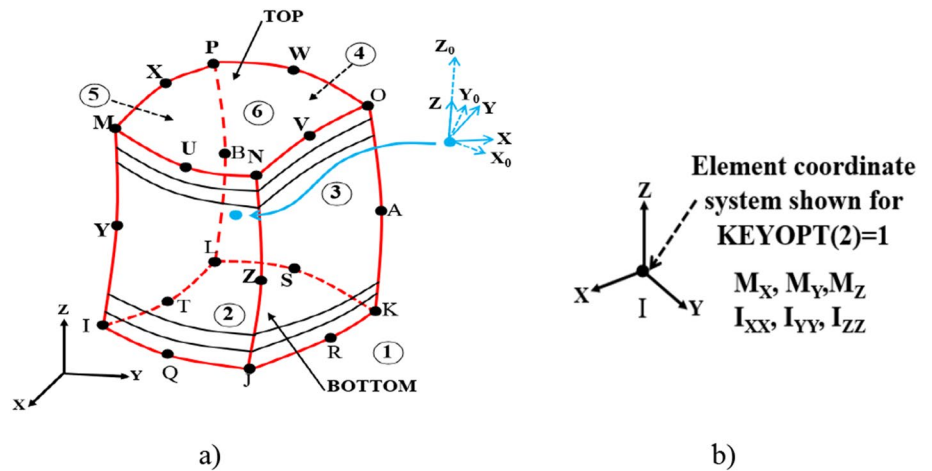


Fig. 2 Geometric properties of a Solid186 layered element and b Mass21 element (ANSYS 2015)



In order to drive the composite manipulator, a revolute joint in the FE model is defined at the root. The MPC184 element is used to specify the revolute joint in ANSYS (2015). The MPC184 element, which is a revolute joint element with two nodes that perform relative rotation around the x and z axes, only allows rotations around the axis of rotation, and also valid kinematic constraints where rotations on other axes are constant. If the settling of the MPC184 element is selected as “KEYOPT(4),1”, the revolute axis

is determined as the z -axis revolute joint. Node locations and geometric properties for the revolute joint element are indicated in Fig. 3.

From Fig. 3, the general coordinate system is defined first at the I node, and a second coordinate system is specified at the J node. The I and J nodes are the ground and body nodes in the FE modeling. The local e_1 and e_3 directions are determined as the rotation axis at the node. The determination of the two local directions defines the relative rotation between

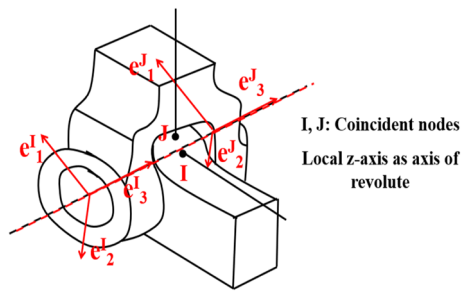


Fig. 3 Geometric properties and node locations of MPC184 element (ANSYS 2015)

the nodes during the movement of the revolute joint. The identifier of local coordinate systems is determined by the “SECJOINT” command in ANSYS. A revolute joint element is then defined between the ground and flexible composite link as the rotation z-axis described by Malgaca and Uyar (2019).

A total of 408 elements and 3324 nodes are used to model the FCM. The FE model is located in a global coordinate system at point A. The geometric and material properties are given in Table 1.

The dimensions are the rectangular cross-section of 20 mm × 3 mm. Two different FCMs, with total length of 363 mm and 500 mm, are selected for transient analysis. The acceleration sensor is located at a distance of 40 mm from the tip point to measure the acceleration signals utilized in the experiment considered in the FE model. In order to take into consideration the flexibility of the gearbox in experiments, the rotational spring coefficient of K_m is selected as

Table 1 Properties of composite manipulator

Composite manipulator		
$\rho = 1510 \text{ kg/m}^3$		
Young's modulus (GPa)	Poisson's ratio	Shear modulus (GPa)
$E_1 = 40.51$	$\nu_1 = 0.22$	$G_1 = 3.1$
$E_2 = 13.96$	$\nu_2 = 0.22$	$G_2 = 3.1$
$E_3 = 13.96$	$\nu_3 = 0.11$	$G_3 = 1.5$
Numerical values		
Lengths, L	363 mm, 500 mm	
Rectangular cross-section, $h \times b$	20 mm × 3 mm	
Distance of sensor from endpoint	40 mm	
Weight of sensor	0.054 kg	
Rayleigh damping coefficients, α, β	0.00171, 0.00085	
Motor rotational spring constant, K_m	16,000 Nm/rad	

16,000 Nm/rad and defined as the revolute joint constant at the general coordinate axis.

Transient analysis is performed to determine the vibration response of structures that are subjected to time-dependent loads, taking into account the damping effects. Rayleigh damping coefficients, which are proportional damping, are used to take into account the damping effect while performing dynamic analysis of the structure. In the transient analysis of the FE model, the damping matrix $[C]$ is calculated from the product of the mass α and stiffness β coefficients as a combination of the mass and stiffness matrices with the following equation

$$[C] = \alpha[M] + \beta[K] \tag{1}$$

where α and β are proportional mass and stiffness damping coefficients in Rayleigh damping. These values are obtained from the experimental vibration responses given in Table 1.

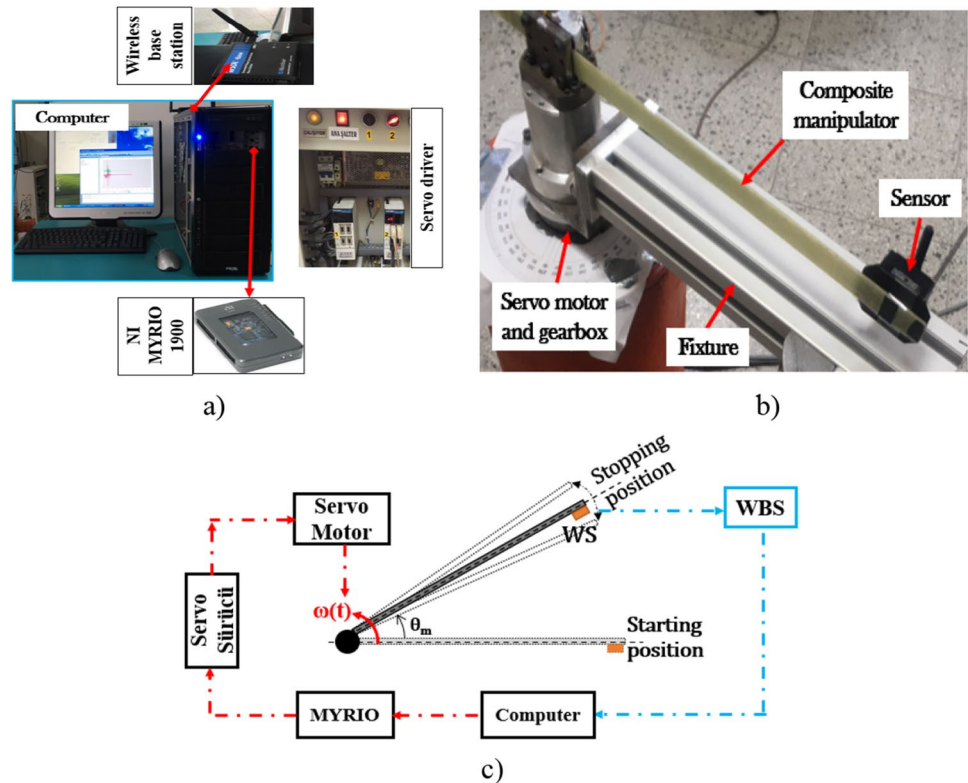
3 Experimental System

Simulation studies in this paper are verified with the experiments. The experimental system with a motion control system and composite manipulator is shown in Fig. 4 in order to carry out the modal and motion-based control analyses.

The experimental system can be described in two parts as the data acquisition phase consisting of the vibration measurement systems and control phase that provide the movement of the manipulator. In the control section, NI MYRIO consists of control card, gearbox, servo motor and driver, while in the data acquisition section, it consists of a wireless acceleration base station (WBS) and acceleration sensor (WS). A personal computer and composite manipulator are used as basic equipment in both parts. In this study, we used a 200W HC-KFS23B model servo motor (Mitsubishi) and MR-J2S-20A model driver (Mitsubishi) and a gearbox (Harmonic Drive) with a transmission ratio of 100. The control card module, which is a multifunction configurable device with analog output/input (O/I) and digital output/input (O/I), is a MYRIO1900 model (National Instruments [NI]). G-link WS and WSDA-101 WBS (Lord Microstrain) are used to experimentally obtain endpoint vibrations. WS can measure maximum and minimum acceleration amplitudes of $\pm 10 \text{ g}$.

Briefly, a program is prepared on the computer by using the LabVIEW program to move the manipulator in the experimental system and to measure the vibrations at the endpoint. In the program, the velocity motion profiles is created parametrically according to angular position and time parameters of three different modified motion profiles. The following connections are made for the control phase: the computer and the control card are connected via USB, control commands are sent to the servo driver using the analog

Fig. 4 Experimental system **a** motion-based control system, **b** composite manipulator, **c** flow chart



output channels of the control card, the servo driver is connected to the servo motor using the SSNET protocol, the connection of the servo motor and the composite manipulator is completed with the help of the gearbox and fixture. Motion control is carried out with an analog speed command by using analog speed control mode in the servo driver. In the speed control mode, motion profiles are converted to 0 to ± 10 VDC and sent to the driver via NI MYRIO hardware to move the manipulator. Also, in the data acquisition phase, the WS placed at the tip point of the manipulator is fixed with a bolt. The measured signals are transmitted by the WS to the WBS by wireless communication. WBS transmits data to a computer via a USB connection. The Lord Microstrain node commander program is used to record and observe the acceleration data.

While the sampling frequencies of the WS can be selected as 50, 100, 256, 512 and 617 Hz, a maximum sampling frequency of 617 Hz is chosen during the data acquisition phase in the experiments. After passing the internal digital filtering processes in the WS to the measured acceleration signals, if needed, a two-order Butterworth low-pass filter with a cut-off frequency of 30 Hz is applied to the recorded acceleration signals to compare the simulation results with the simulation results. While determining the cut-off frequency, attention is paid to ensure that there is no data loss in the acceleration signals and is determined according to the natural frequencies of the manipulators. In order to obtain

accurate results during the comparison of experimental results, the weight of the acceleration sensor placed at the end of the manipulator is defined as the payload to the finite element model in ANSYS.

In the experiments, moving the manipulator and acquiring the endpoint vibration signals are performed simultaneously. The high-performance computers are closely monitored during the data acquisition phase of the experiments in order to prevent the shifts and delays in the time steps. The reliability of the vibration responses obtained for each motion profile is verified by a reproducible number of experiments. In this study, experiments are carried out for motion-based vibration control using three different modified motion profiles of two different lengths of composite manipulators.

4 Motion-Based Control

Various velocity profiles are used to drive the flexible and rigid manipulators. Trapezoidal velocity profiles are the most common motion profiles used for manipulators. The effect of the values of the time parameters of the motion profiles on the endpoint vibrations of the manipulators is a common research topic. In the studies in this paper, a motion-based control (MBC) application is implemented with three different newly modified trapezoidal motion

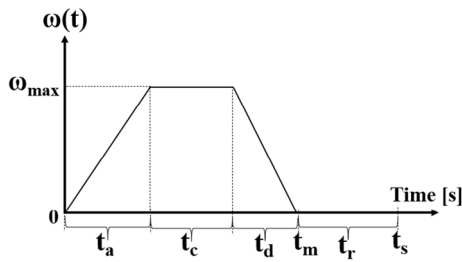


Fig. 5 Trapezoidal motion profile

profiles to reduce extreme vibrations. An example trapezoidal motion profile is shown in Fig. 5.

From Fig. 5, the trapezoidal motion profile occurs at the values of time parameters and maximum angular velocity. t_a , t_c , t_d values from time parameters are represented as the acceleration, constant, and deceleration time values, respectively, while t_m , t_r , and t_s are specified as the motion, residual, and settling time values in the trapezoidal motion profile. In addition, ω_{max} is the maximum angular velocity. Since the natural frequencies are used to determine the time and angular velocity values of the motion profile, firstly, the modal analysis results of the two different lengths of the FCM are examined.

4.1 Modal Analysis

Modal analysis is carried out to determine the natural frequencies and mode shapes that are considered during the simulation and experimental studies, before determining the modified motion profiles. For the dynamic vibration analysis of the FCM, the experimental modal analysis is performed by considering both the impact test results applied to the endpoint of the composite link from different directions and the residual vibration results generated at the endpoint as a result of driving the composite manipulator with varying profiles of motion. Frequency and amplitude results are obtained by applying fast Fourier transform (FFT) to vibration responses. Thus, experimental modal analysis is

performed. In order to determine whether the dynamic characteristics of the FE model are compatible with the experiments, the experimental modal analysis results are compared with the simulation results. Therefore, modal analysis is performed with the FE analysis in ANSYS to obtain the results of the modal analysis numerically. Experimental and simulation modal analysis results for two different composite manipulators are presented in Table 2.

The first three mode shapes and dynamic behaviors of modal analysis results, in which the dynamic properties of the structure are determined, are shown in Fig. 6.

The dynamic properties of the system provide basic information about whether the numerical model of a structure is modeled correctly. For modal analysis results, the FE model validation is done with the experimental studies using the frequency and amplitude responses. Therefore, as a result of the modal analysis, when the results are investigated, it is clear that the natural frequencies of two different composite manipulators are coherent and very close to each other.

For the transient analysis, the time parameters are determined as $t_s = t_r + t_m$ and the time step dt is chosen as $dt = 1/f_1/20$ s. f_1 is the first natural frequency of the composite manipulators in the bending direction.

4.2 Modified Motion Profiles

Studies of MBC have generally examined the effect of deceleration time on motion profiles. In this study, three different modified trapezoidal motion profiles given in Fig. 5 are investigated to examine the effect of variation of the acceleration, constant, and deceleration times. The modified motion profiles are shown in Fig. 7.

In Fig. 7, the variation of the time parameters of the modified motion profiles, named Modification-1, Modification-2, and Modification-3, is shown as a schematic view. Briefly, for Modification-1, the time and velocity parameters of motion profiles are calculated using the following equations

Table 2 Natural frequencies of FCM

Order of natural frequency	L = 363 mm		L = 500 mm	
	Simulation (Hz)	Experiment (Hz)	Simulation (Hz)	Experiment (Hz)
f_1	6.839	6.850	4.173	4.187
f_2	45.804	46.920	28.011	29.952
f_3	82.004	84.307	44.538	46.025

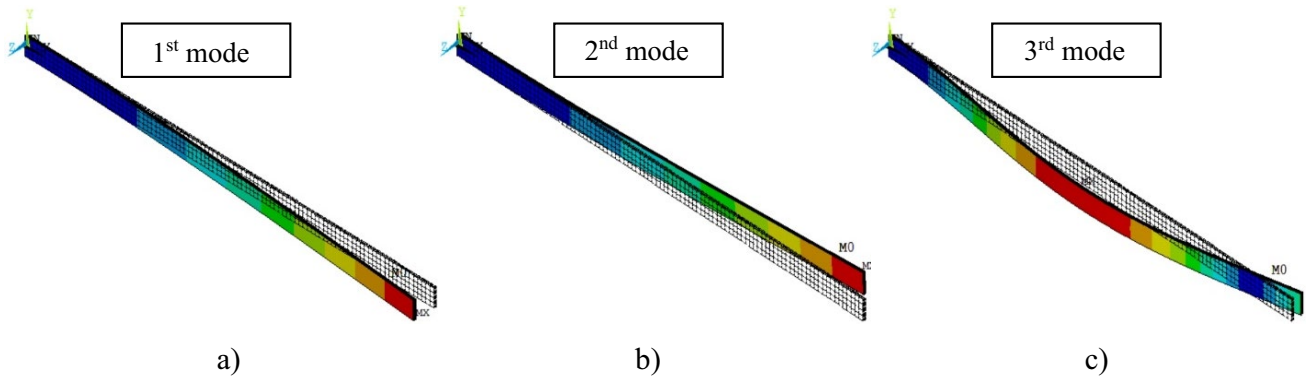


Fig. 6 Mode shapes of the FCM with length of $L=500$ mm

$$\begin{aligned}
 t_n &= 1/f_1/2 \\
 w_d &= 2\pi f_1 \sqrt{1-\zeta^2} \quad \zeta = 0.1, 0.2, 0.3, \dots 0.9 \\
 t_d &\rightarrow \begin{cases} r_z = 1 & t_d = \pi/w_d \\ r_z = 2 & t_d = 2\pi/w_d \\ r_z = 3 & t_d = 3\pi/w_d \end{cases} \\
 t_c &= r_c t_n \\
 t_a &= t_m - t_c - t_d \\
 \omega_{\max} &= \frac{\theta_m}{0.5(t_a + t_d) + t_c}
 \end{aligned} \tag{2}$$

where t_d values are found with r_z and w_d changes depending on the first natural frequency of the FCM. r_z takes values of 1, 2, 3, while ζ varies between 0.1 and 0.9 in increments of 0.1. In the motion profile for Modification-1, the r_c value is taken as 0 or 2. If the r_c value is taken as $rc=0$, the motion profile is considered as a triangular velocity profile, and when the r_c value is taken as $rc=2$, it is the trapezoidal motion profile. Also, in Eq. (2), ω_{\max} and θ_m are determined as the maximum angular velocity and stopping position, respectively. For Modification-1, as t_d values increase for each motion profile, t_a values decrease and t_c values are the constant. Secondly, the time and velocity parameters of the

modified motion profile for Modification-2 are calculated using the following equations

$$\begin{aligned}
 t_n &= 1/f_1/2 \\
 t_d &= \left(\frac{t_m}{2}\right) - r_n t_n \quad r_n = 0, 0.5, 1, 1.5, \dots \\
 t_c &= t_m - 2t_d \\
 t_a &= t_d \\
 \omega_{\max} &= \frac{\theta_m}{0.5(t_a + t_d) + t_c}
 \end{aligned} \tag{3}$$

In Modification-2, t_d , t_c and t_a values of the time parameters are calculated as defined in the equation above, depending on the variation of the natural frequency and r_n values. The variable r_n starts from 0 and increases by 0.5 to get the maximum value it can take, and the effect of the motion-based vibration control depending on the change of r_n values is examined. For Modification-2, t_a and t_d values are considered equal, while t_c values vary for each motion profile according to t_a and t_d values. As t_d and t_a values for Modification-2 decrease, t_c values for each motion profile increase. Finally, motion parameters for Modification-3 are obtained using the following equations

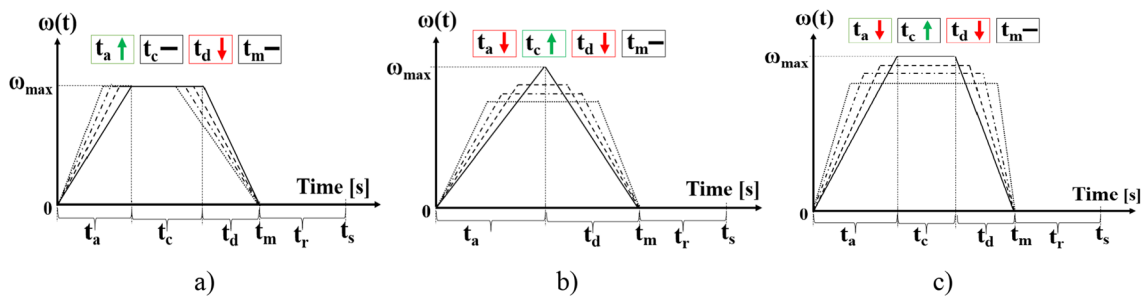


Fig. 7 Modified trapezoidal motion profiles: **a** Modification-1, **b** Modification-2, and **c** Modification-3

$$\begin{aligned}
 t_n &= 1/f_1/2 \\
 w_d &= 2\pi f_1 \sqrt{1-\zeta^2} \quad \zeta = 0.1, 0.2, 0.3, \dots 0.9 \\
 t_d &\rightarrow \begin{cases} r_z = 1 & t_{1m} = \pi/w_d \\ r_z = 2 & t_{1m} = 2\pi/w_d \\ r_z = 3 & t_{1m} = 3\pi/w_d \end{cases} \\
 t_d &= \left(\frac{t_m}{2}\right) - t_{1m} \\
 t_c &= t_m - 2t_d \\
 t_a &= t_d \\
 \omega_{\max} &= \frac{\theta_m}{0.5(t_a + t_d) + t_c}
 \end{aligned}
 \tag{4}$$

From Eq. 4, in general, Modification-3 motion profiles consist of a combination of Modification-1 and Modification-2. Motion parameters for Modification-3 are found using these equations. Parameters of the motion profile for Modification-3 are determined as in Modification-1 depending on the variation of r_z and ζ values. However, there is a difference in the calculation of t_d , t_a and t_d values according to Modification-2. The values of the t_a and t_d parameters are equal. The t_c value changes according to the t_d value in each motion profile. Briefly, as the t_d and t_a values decrease in each motion profile in Modification-3, the t_c values increase.

The values of t_m and θ_m parameters are constant in motion profiles. t_a , t_c , t_d and ω_{\max} values vary according to the modification type of the motion profiles: Modification-1, Modification-2, and Modification-3. In the motion profiles created according to the modification types, motion profiles occurred according to Modification-2 and Modification-3 generally consist of the trapezoidal motion profiles, while the motion profiles of Modification-2 transform into the trapezoidal motion profiles from the triangular motion profiles due to the change in the values of time and velocity parameters.

Time and angular velocity parameters are calculated with the above equations. Motion profiles are created using the equation given below at defined time intervals depending on the variables. Thus, the velocity profile is applied to the revolute joint of the FE model for the simulation results, while the motion profiles given in Eq. 5 are created in the LabVIEW program in experimental studies and applied to the experimental system as an angular velocity profile.

$$\omega(t) \rightarrow \begin{cases} t = 0 : dt : t_s & \\ \frac{\omega_{\max} * t}{t_a} & 0 < t < t_a \\ \omega_{\max} * t & t_a < t < t_a + t_c \\ \omega_{\max} - \frac{\omega_{\max} * (t - t_a - t_c)}{t_d} & t_a + t_c < t < t_m \\ 0 & t_m < t < t_r \end{cases}
 \tag{5}$$

where dt is the step time, and $\omega(t)$ is the value of time-dependent angular velocity profiles. The manipulator drives from a starting position (at 0° , $t = 0$ s) to a stopping position (at θ_m° , $t = t_m$ s).

5 Motion Control Analysis

In this section of the paper, the experimental and numerical analyses are performed using three different modified motion profiles. According to the formal design shown in Fig. 8, MBC is performed by considering Modification-1, Modification-2, and Modification-3 motion profiles.

Velocity profiles prepared from Modification-1, Modification-2, and Modification-3 motion profiles are applied to the revolute joint of the FE model for simulation results using a computer, and transmitted to the servo driver for experimental results. The composite manipulator reaches from the starting position to the stopping position during the motion time. After the manipulator has completed its movement, the vibrations occurring at the endpoint are obtained with the acceleration sensor in the experimental system, while in the FE analysis, the rigid body motion (RBM) is subtracted from the flexible body motion (FBM) signal and residual acceleration vibration (RAS) results are obtained for all motion profiles.

For all modifications, the motion profiles with two different angular positions of $\theta_m = 60^\circ$ and $\theta_m = 75^\circ$, and motion times of 1 s and 1.5 s are studied. The FCM is considered in order to verify the simulation results with the experiments. The results obtained as a result of all analysis are examined in detail in the following sections.

5.1 Residual Vibration Results

For three various modified motion profiles, two different lengths of the composite manipulators are taken into account for the motion-based vibration control in the simulation and experimental studies, while the analysis results are obtained for the stopping position of $\theta_m = 60^\circ$ and the motion time of

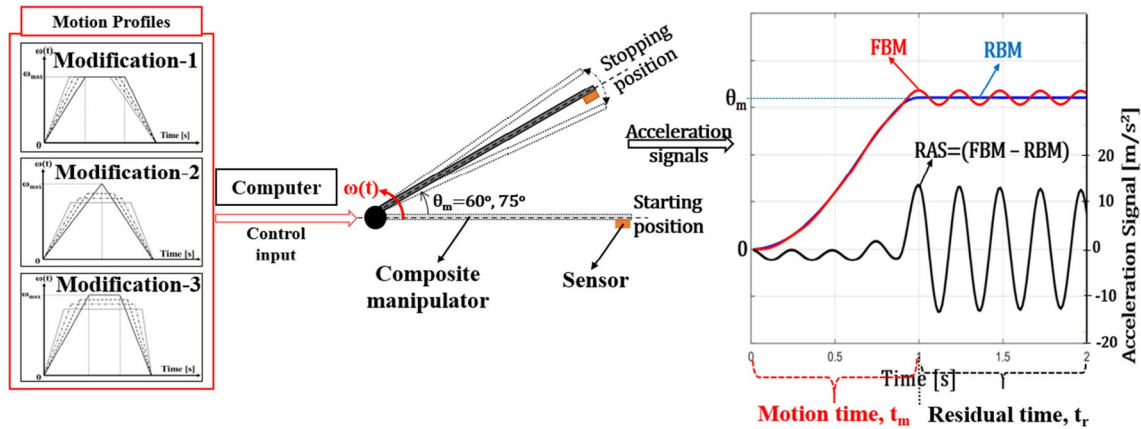


Fig. 8 Detailed information about MBC

$t_m = 1$ s for the length $L = 363$ mm of the composite manipulator, the results are achieved for $\theta_m = 75^\circ$ and $t_m = 1.5$ s to examine the effect of the length $L = 500$ mm of the FCM on the different stopping positions and modified motion profiles in MBC. For $\theta_m = 75^\circ$ and $t_m = 1.5$ s, three different example simulation and experimental vibration responses for Modification-1, Modification-2, and Modification-3 motion profiles are shown in Fig. 9.

For the FCM, Fig. 9 indicates the experimental and simulation vibration responses of the MBC with three different modified motion profiles. In the simulation results, the endpoint vibrations are found by measuring the vibrations generated by subtracting the flexible body motion from the rigid body motion of the composite manipulator. Verification of vibration responses provides important information about whether the numerical model of the mechanical system is correct. In this study, the vibration responses of the composite manipulator are obtained from both experiments and numerical methods. As can be seen from Fig. 9, it can be seen that the simulation results match well with the experiments. With the verification of the vibration responses, it is clear that the FE model of the composite manipulator is modeled correctly. It is observed that the amplitudes of the vibration responses are not equal for each motion profile and differ according to the velocity profiles. The reduction rates of endpoint vibration responses are an effective evaluation criterion to interpret the effect of MBC implementation on the composite manipulators. The reduction ratios are calculated using the root mean square (RMS) values of the vibrations occurring at the tip point of the composite manipulator. The residual vibration responses of the FCM are taken into account for the RMS values. Vibrations that occur after the motion time t_m when the composite manipulator completes its movement are residual vibrations, also, where the residual time of vibration response is defined as t_r .

The RMS values of each motion profile are calculated from the residual vibrations. Using RMS values, the reduction rates are obtained to examine the effectiveness of motion-based vibration control. In order to evaluate the efficiency of the modified motion profiles, the vibration responses received at the values of $r_z = 1$ and $\zeta = 0.1$ in the Modification-1 motion profile are accepted as reference values in calculating the reduction ratios of the vibration responses. RMS values and reduction rates obtained from residual vibration responses are listed in Tables 3, 4 and 5 for Modification-1, Modification-2 and Modification-3 motion profiles, respectively.

Tables 3, 4 and 5 give the results of RMS and reduction ratios of the FCM obtained using Modification-1, Modification-2, and Modification-3 motion profiles, respectively. For the MBC, the vibration amplitudes for $\theta_m = 60^\circ$ and $t_m = 1$ s are reduced by Modification-1 from 7.8974 m/s², 7.6358 m/s² to 0.5386 m/s², 0.6335 m/s², while those values for $\theta_m = 75^\circ$ and $t_m = 1.5$ s are diminished from 6.5721 m/s², 6.4179 m/s² to 0.1614 m/s², 0.1716 m/s², for the simulation and experimental studies, respectively. Minimum vibration amplitudes for the simulation and experimental results are obtained as 0.1940 m/s², 0.1577 m/s² for Modification-2, and 0.0352 m/s², 0.0373 m/s² for Modification-3, separately.

The simulation and experimental results of Modification-1, Modification-2, and Modification-3 motion profiles, depending on the motion parameters, are shown in Figs. 10, 11 and 12 to observe the change of RMS values.

In the figures above, the endpoint acceleration vibration responses for Modification-1 in Fig. 10, Modification-2 in Fig. 11, and Modification-3 in Fig. 12 are given during and after the movement of the composite manipulator. Experimental and simulation studies are carried out at different motion parameters and angular velocities for three different modified motion profiles defined in the previous section. As seen from the figures, it is clear that the simulation

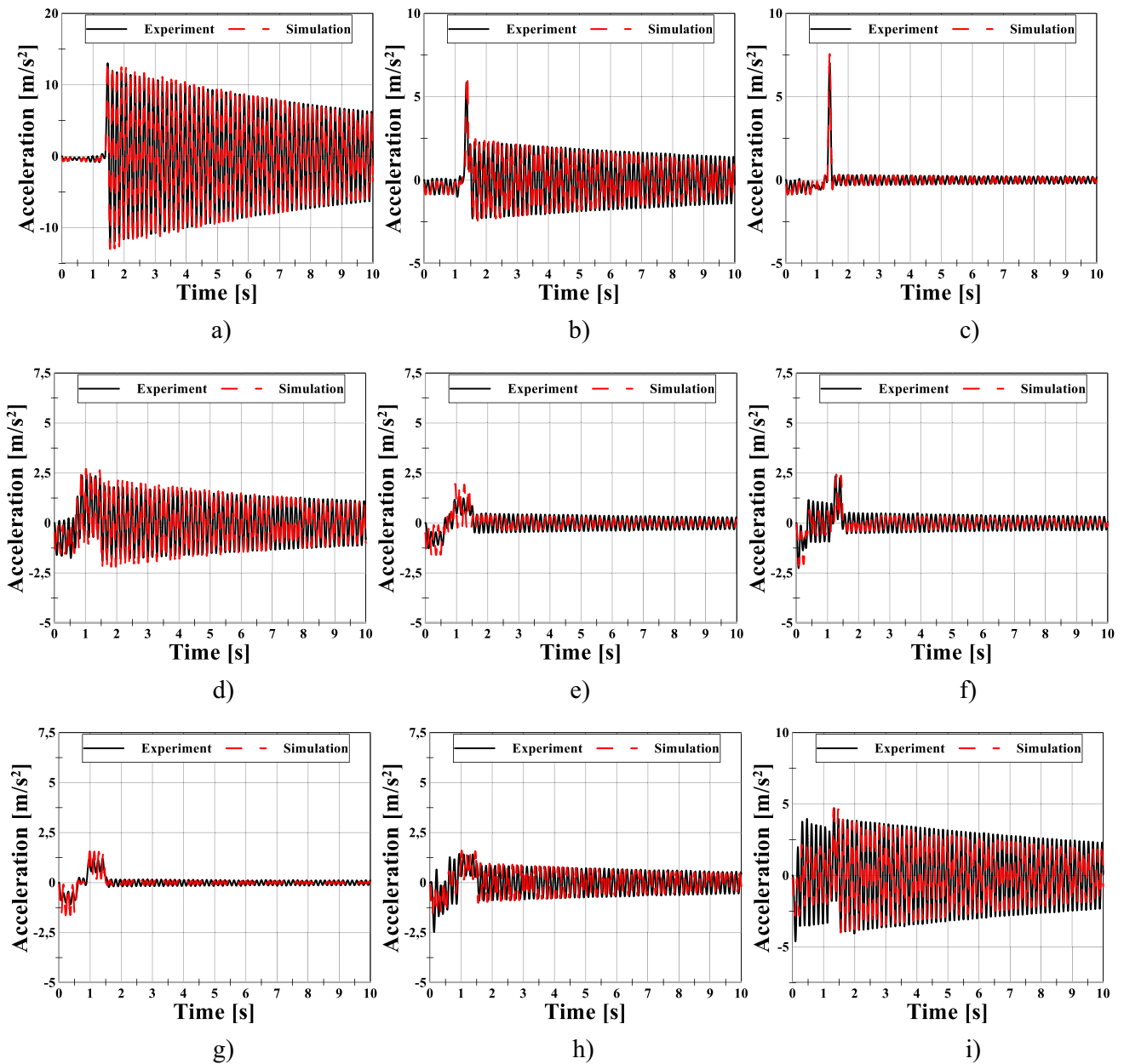


Fig. 9 Example time history vibration amplitudes of simulation and experimental studies for $\theta_m = 75^\circ$ and $t_m = 1.5$ s, **a–c** Modification-1, **d–f** Modification-2, **g–i** Modification-3

results are matched well with the experimental results for two different angular positions, motion times, and composite manipulators. From the figures, the change in RMS values in the vibration results obtained for two different angular positions are similar in shape for each modified motion profile. Generally, when evaluating the RMS values for comparison, while maximum acceleration amplitudes occur in the Modification-1 motion profile, minimum vibration amplitudes are obtained for each configuration at approximately the same values.

5.2 Performance Comparison of Modified Motion Profiles

In this section, we examine the results of the transient simulation analysis and experimental studies and discuss the effectiveness of the change in the RMS values in the previous section on the reduction of endpoint vibrations. Depending on the time and velocity parameters of all modified motion profiles, the reduction rates are obtained. In determining the reduction ratios, the RMS values are subtracted

Table 3 RMS values and reduction ratios for Modification-1

Motion parameters						RMS value		Reduction ratio (%)		
r_c	r_z	ζ	t_m	θ_m , degrees	ω_{\max} (rad/s)	Simulation	Experiment	Simulation	Experiment	
2	1	0.1	1	60	1.6907	7.8974	7.6358	–	–	
		0.2				7.4025	7.1975	6.27	5.74	
		0.4				7.0134	7.0255	11.19	7.99	
		0.6				6.0343	5.8812	23.59	22.98	
		0.8				2.3866	1.6348	69.78	78.59	
		0.9				1.1928	1.3013	84.90	82.96	
		2				0.1	0.6530	0.4980	91.73	93.48
						0.2	0.5386	0.6335	93.18	91.70
						0.4	0.5609	0.6239	92.90	91.83
	3	0.1	0.4	2.2942	2.5585	70.95	66.49			
			0.6	2.2942	2.5585	70.95	66.49			
			0.8	3.8567	3.7164	51.16	51.33			
		0.2	0.9	2.3428	2.1991	70.33	71.20			
			0.1	3.8484	3.8433	51.27	49.67			
			0.2	3.9060	3.9496	50.54	48.28			
		0.4	0.6	3.9058	3.9442	50.54	48.35			
			0.8	2.5998	2.5112	67.08	67.11			
			0.9	5.2529	5.4042	33.49	29.23			
2	1	0.1	1.5	75	1.5904	6.5721	6.4179	–	–	
		0.3				6.2952	6.0842	4.21	5.20	
		0.4				6.0784	5.9022	7.51	8.04	
		0.6				4.9743	4.8658	24.31	24.18	
		0.8				2.1927	2.3701	66.64	63.07	
		0.9				1.1950	1.2533	81.82	80.47	
		2				0.1	0.1614	0.1716	97.54	97.33
						0.3	0.4269	0.5275	93.50	91.78
						0.4	0.8351	0.9022	87.29	85.94
	3	0.6	1.8588	2.1247	71.72	66.89				
			0.8	1.9326	1.7970	70.59	72.00			
			0.9	1.1642	1.3030	82.29	79.70			
		0.1	0.1	2.3438	2.4581	64.34	61.70			
			0.3	2.2296	2.3562	66.07	63.29			
			0.4	2.0488	2.0465	68.83	68.11			
		0.6	0.6	0.8922	0.8778	86.42	86.32			
			0.7	0.3554	0.4126	94.59	93.57			
			0.8	1.5196	1.5694	76.88	75.55			
	0.9	1.2560	1.5008	80.89	76.62					

from the reference RMS value and then divided by the reference value and multiplied by 100. When the reference RMS values are accepted, the RMS values of the vibration responses occurring in the $r_z=1$ and $\zeta=0.1$ parameters of Modification-1 motion profile for each angular position and motion times, and where the maximum acceleration values are obtained, are taken into account. The reduction ratios calculated for motion profiles, where the effect of motion-based vibration control is investigated, are shown in Fig. 13 for Modification-1.

In the figure, the reduction rates of residual vibrations at the endpoint of the composite manipulator for each time and

speed parameter values of the Modification-1 motion profile are shown in comparison with the experimental and simulation results. The maximum reduction ratio for $\theta_m=60^\circ$ and $t_m=1$ s is about 97.12% for $r_z=2$ and $\zeta=0.3$, while this value for $\theta_m=75^\circ$ and $t_m=1.5$ s is obtained as 97.54% for $r_z=2$ and $\zeta=0.1$. As seen from Fig. 13a, the rate decrease increases as the ζ values for $r_z=1$ increase. However, a linear connection cannot be established with the rate of growth and decrease of ζ values for $r_z=2$ and $r_z=3$ values, and it is clear that it varies according to the parameters. In addition, when the FCM is driven with the parameter values $r_z=2$ and between $\zeta=0.1$ –0.4, the endpoint vibrations are almost

Table 4 RMS values and reduction ratios for Modification-2

Motion parameters				RMS value		Reduction ratio (%)	
r_n	t_m	θ_m , degrees	ω_{max} (rad/s)	Simulation	Experiment	Simulation	Experiment
0	1	60	2.0944	0.3543	0.3730	95.51	95.12
1			1.6907	3.9479	3.8735	50.01	49.27
1.5			1.5420	2.2180	2.4459	71.91	67.97
2			1.4174	0.2098	0.1577	97.34	97.93
2.5			1.3114	2.8353	3.0097	64.10	60.58
3			1.2202	6.2023	6.0566	21.46	20.68
0	1.5	75	1.7453	0.2160	0.3918	96.71	93.90
0.5			1.6643	0.4400	0.4504	93.31	92.98
1			1.5904	1.0031	1.0905	84.74	83.01
2			1.4607	0.1940	0.2688	97.05	95.81
2.5			1.4035	0.4804	0.4281	92.69	93.33
3			1.3506	1.0821	1.0462	83.53	83.70
3.5			1.3016	0.5219	0.5101	92.06	92.05
4			1.2559	0.2062	0.4078	96.86	93.65
4.5			1.2134	0.2802	0.3127	95.74	95.13
5			1.1737	1.4511	1.4577	77.92	77.29
5.5			1.1364	0.5861	0.5491	91.08	91.44
6			1.1015	0.2521	0.2858	96.16	95.55
6.5			1.0687	0.5523	0.6014	91.60	90.63

Table 5 RMS values and reduction ratios for Modification-3

Motion parameters						RMS values		Reduction ratios (%)	
r_c	r_z	ζ	t_m	θ_m , degrees	ω_{max} (rad/s)	Simulation	Experiment	Simulation	Experiment
2	1	0.1	1	60	1.6890	3.9485	4.0862	50.00	46.49
		0.4			1.6615	3.9079	3.8633	50.52	49.41
		0.6			1.6129	2.9929	2.9670	62.10	61.14
		0.9			1.3531	0.9660	1.0310	87.77	86.50
	2	0.1			1.4151	0.4058	0.9089	94.86	88.10
		0.4			1.3769	0.0352	0.0373	99.55	99.51
		0.6			1.3114	2.8353	2.9113	64.10	61.87
		0.8			1.1661	7.4709	7.2894	5.40	4.54
	3	0.1			1.2177	6.6349	6.8960	15.99	9.69
		0.4			1.1755	7.7835	7.4231	1.44	2.79
		0.5			1.1462	6.2043	6.0621	21.44	20.61
2	1	0.1	1.5	75	1.5897	0.7989	0.7875	87.84	87.73
		0.3			1.5836	0.6703	0.6127	89.80	90.45
		0.6			1.5559	0.9076	0.8960	86.19	86.04
		0.9			1.4265	0.0595	0.1023	99.09	98.41
	2	0.1			1.4595	0.1986	0.1900	96.98	97.04
		0.3			1.4493	0.1728	0.2551	97.37	96.03
		0.4			1.4394	0.0603	0.0725	99.08	98.87
		0.6			1.4035	0.4785	0.4833	92.72	92.47
		0.8			1.3175	0.7760	0.8117	88.19	87.35
	3	0.1			1.3491	1.1905	1.1667	81.89	81.82
		0.3			1.3360	1.1314	1.1231	82.78	82.50
		0.6			1.2783	0.0544	0.2851	99.17	95.56
		0.9			1.0448	1.9046	2.1183	71.02	66.99

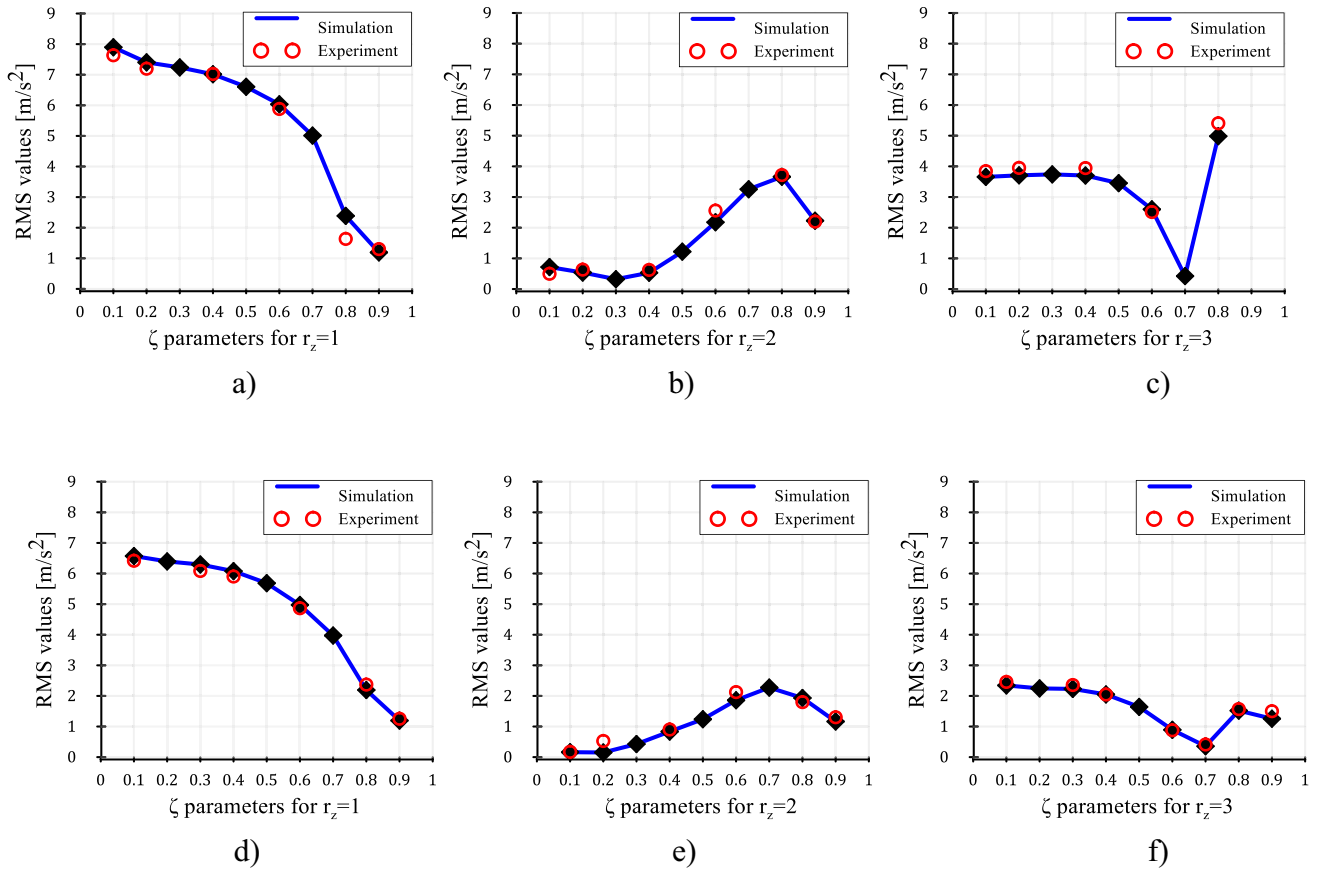
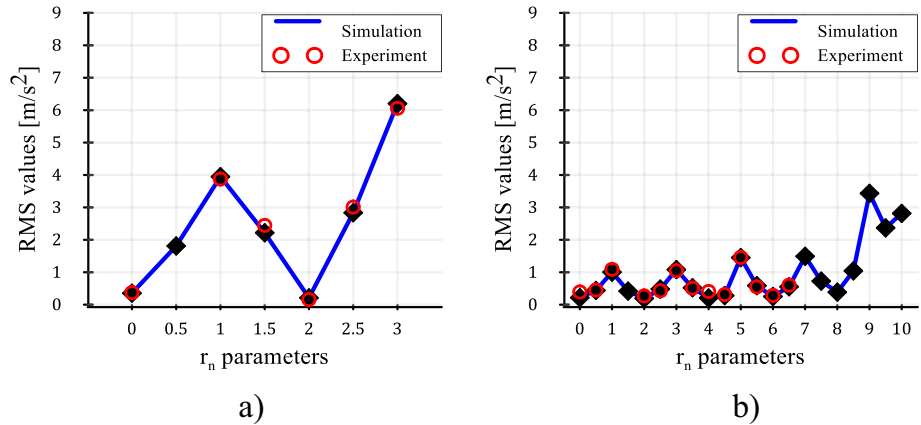


Fig. 10 Change of RMS values of time history acceleration responses for Modification-1, a–c $\theta_m=60^\circ$ and $t_m=1$ s, d–f $\theta_m=75^\circ$ and $t_m=1.5$ s

Fig. 11 Change of RMS values of time history acceleration responses for Modification-2, a $\theta_m=60^\circ$ and $t_m=1$ s, b $\theta_m=75^\circ$ and $t_m=1.5$ s



negligible, and additionally, for the tasks to be performed, if $r_z=2$ and $r_z=3$ values are used in modeling the motion profiles with Modification-1 to drive the manipulators, it is clear that the endpoint vibrations will be much less than with $r_z=1$ value.

For Modification-2, the reduction ratios for two different stopping positions and motion times are indicated in Fig. 14.

Figure 14 indicates the change in the reduction in vibration amplitudes of the driven FCM with the motion profiles created depending on the time parameters. Since the change of the r_n parameter for Modification-2 depends on the first natural frequency of the manipulator in the bending direction and the movement time, as given in Eq. 3, and also because simulation and experimental studies are carried out for two different motion times of composite manipulators, in

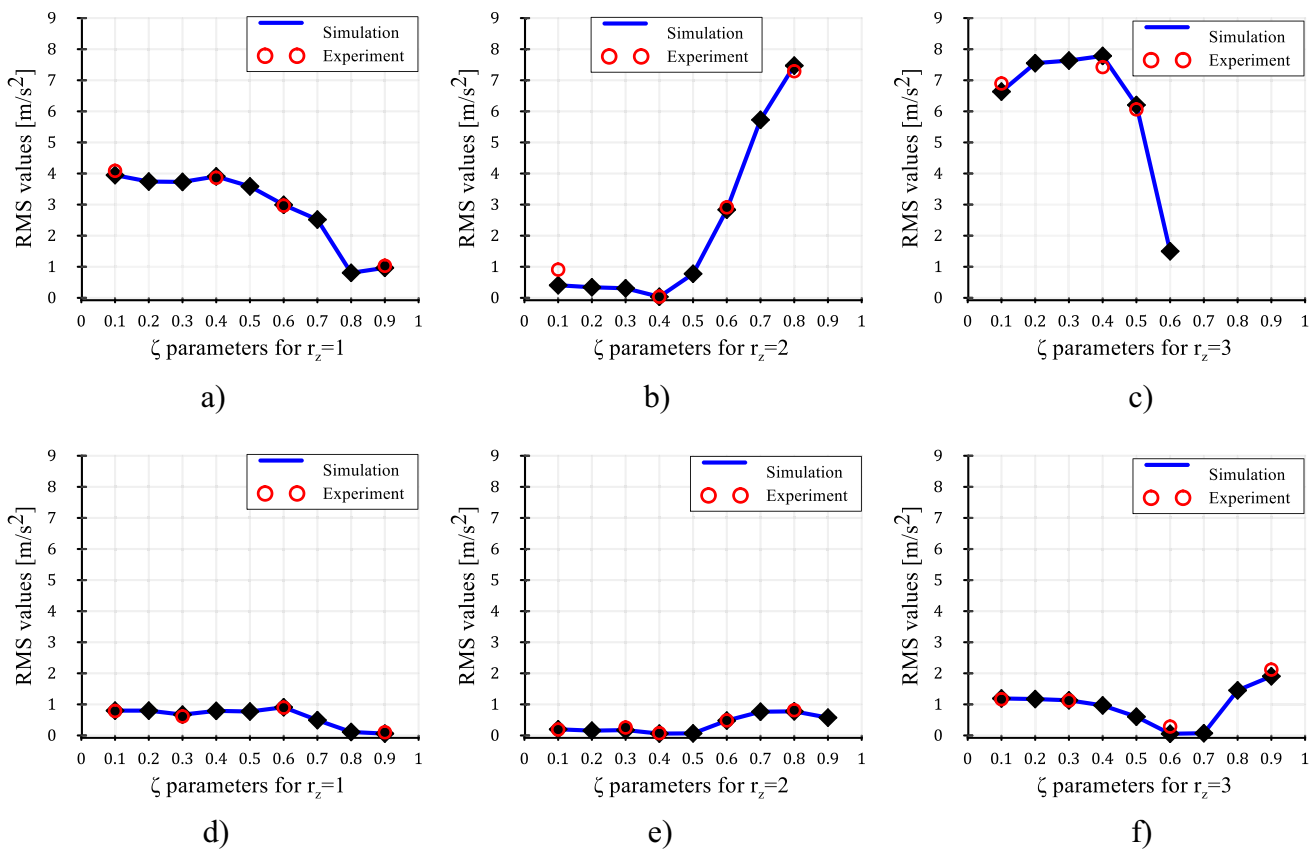


Fig. 12 Change of RMS values of time history acceleration responses for Modification-3, a–c $\theta_m = 60^\circ$ and $t_m = 1$ s, d–f $\theta_m = 75^\circ$ and $t_m = 1.5$ s

determining the maximum limits of r_n values, there are also differences in the maximum r_n values for two different angular positions. In addition, the maximum r_n value is taken as 3 for $\theta_m = 60^\circ$, $t_m = 1$ s and 10 for $\theta_m = 75^\circ$, $t_m = 1.5$ s, respectively. From Fig. 14, it is clear that the results of simulation and experiment are in good agreement. For Modification-2 and angular position of 60° , the rates of reduction of residual endpoint vibrations are experimentally about 95%, 50%, 68%, 98%, 61% and 21% for $r_n = 0, 1, 1.5, 2, 2.5,$ and 3, respectively. In addition, for $\theta_m = 60^\circ$, $t_m = 1$ s, the highest two acceleration reduction values obtained are 95.51%, 97.37% in the simulation and 95.12%, 97.93% in the experiment for $r_n = 0$ and two time parameters, while these values for $\theta_m = 75^\circ$, $t_m = 1.5$ s are 97.05%, 96.16% in the simulation and 95.81%, 95.55% in the experiment for time parameters of $r_n = 2$ and 6, respectively. As a result of the analysis, motion profiles configured with Eq. 3 given in Sect. 4.2 are created at different angular velocities depending on each time parameter. The vibration behavior of FCM at different angular velocities for two different stopping positions is investigated with Modification-2. When comparing the change of the maximum angular velocity and reduction ratios in Modification-2, it is observed that although the maximum angular velocity value decreased while the

time parameter increased in the modified motion profile, the amount of decrease in the vibration amplitudes did not change at the same rate.

The reduction ratios computed for Modification-3 motion profile in the motion-based vibration control are shown in Fig. 15.

Figure 15 also includes comparative results for reduction ratios of the simulation and experimental vibration responses for Modification-3 given in Table 5. Simulation and experimental studies are carried out due to the excess of the parameter values limiting the motion profile for r_z and ζ values for all time parameters of Modification-3 motion profiles created depending on the natural frequency and stopping position of the FCM. For example, the results for $r_z = 3$ and $\zeta = 0.7, 0.8, 0.9$ values for Modification-3 shown in Fig. 15c are not obtained due to limitations such as motion time and constant times. Also, as in Modification-2, the maximum angular velocities of each velocity profile for Modification-3 vary according to the time parameters. From Fig. 15, for $\theta_m = 60^\circ$ and $t_m = 1$ s, the maximum and minimum reductions in residual vibrations are 99.55% for $r_z = 2$ and $\zeta = 0.4$, and 1.44% for $r_z = 3$ and $\zeta = 0.4$ in the simulation, and these values are 99.51% and 2.79% in the experimental studies, respectively. For $\theta_m = 75^\circ$ and $t_m = 1.5$ s, maximum and

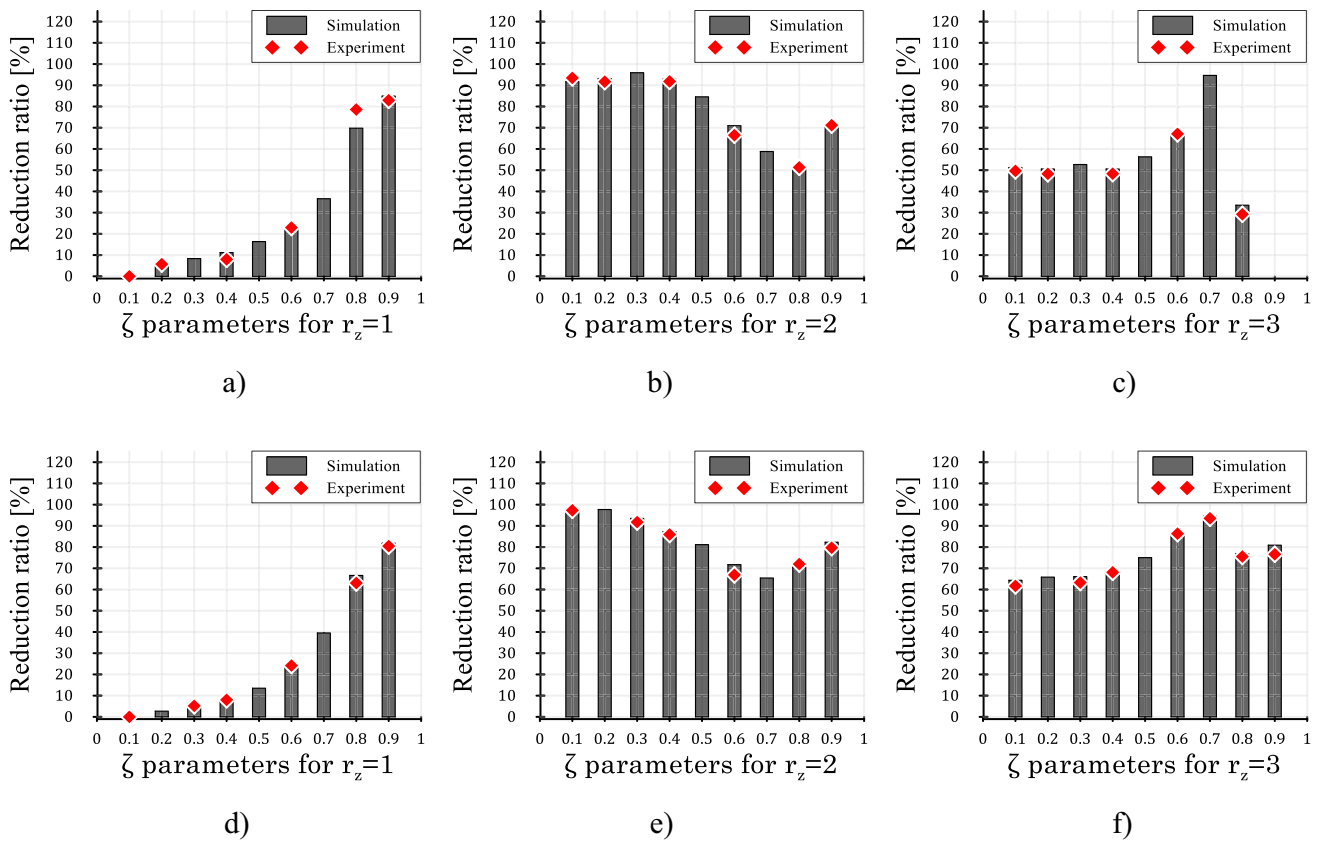
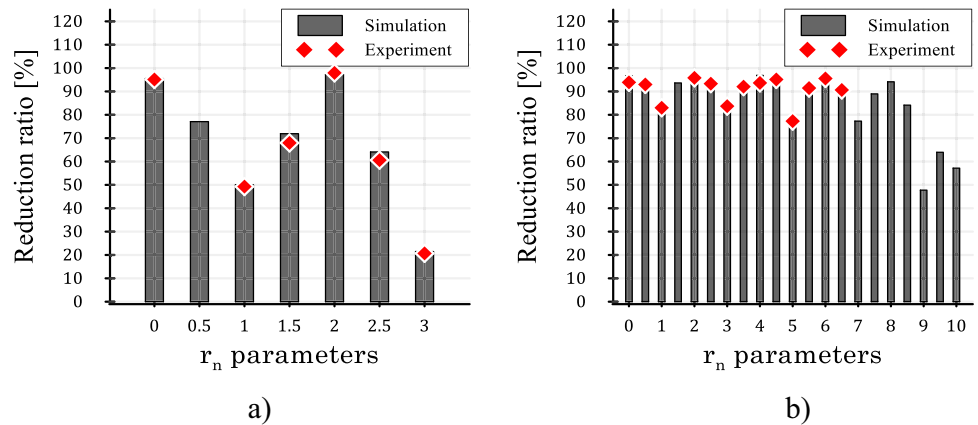


Fig. 13 Reduction ratios according to time parameters of time history acceleration responses for Modification-1, **a-c** $\theta_m = 60^\circ$ and $t_m = 1$ s, **d-f** $\theta_m = 75^\circ$ and $t_m = 1.5$ s

Fig. 14 Reduction ratios according to time parameters of time history acceleration responses for Modification-2, **a** $\theta_m = 60^\circ$ and $t_m = 1$ s, **b** $\theta_m = 75^\circ$ and $t_m = 1.5$ s



minimum reduction ratios obtained are 99.08% and 71.02% for the simulation, and 98.87% and 66.99% for the experiment, respectively. When evaluating the rates of reduction for comparison, the results for Modification-3 indicate that better reduction ratios can be obtained at different time

parameter values, not for a certain time and parametric velocity values.

When the reduction ratio results given in Fig. 15 are compared, it is observed that similar reduction ratios are obtained for composite manipulators with different natural

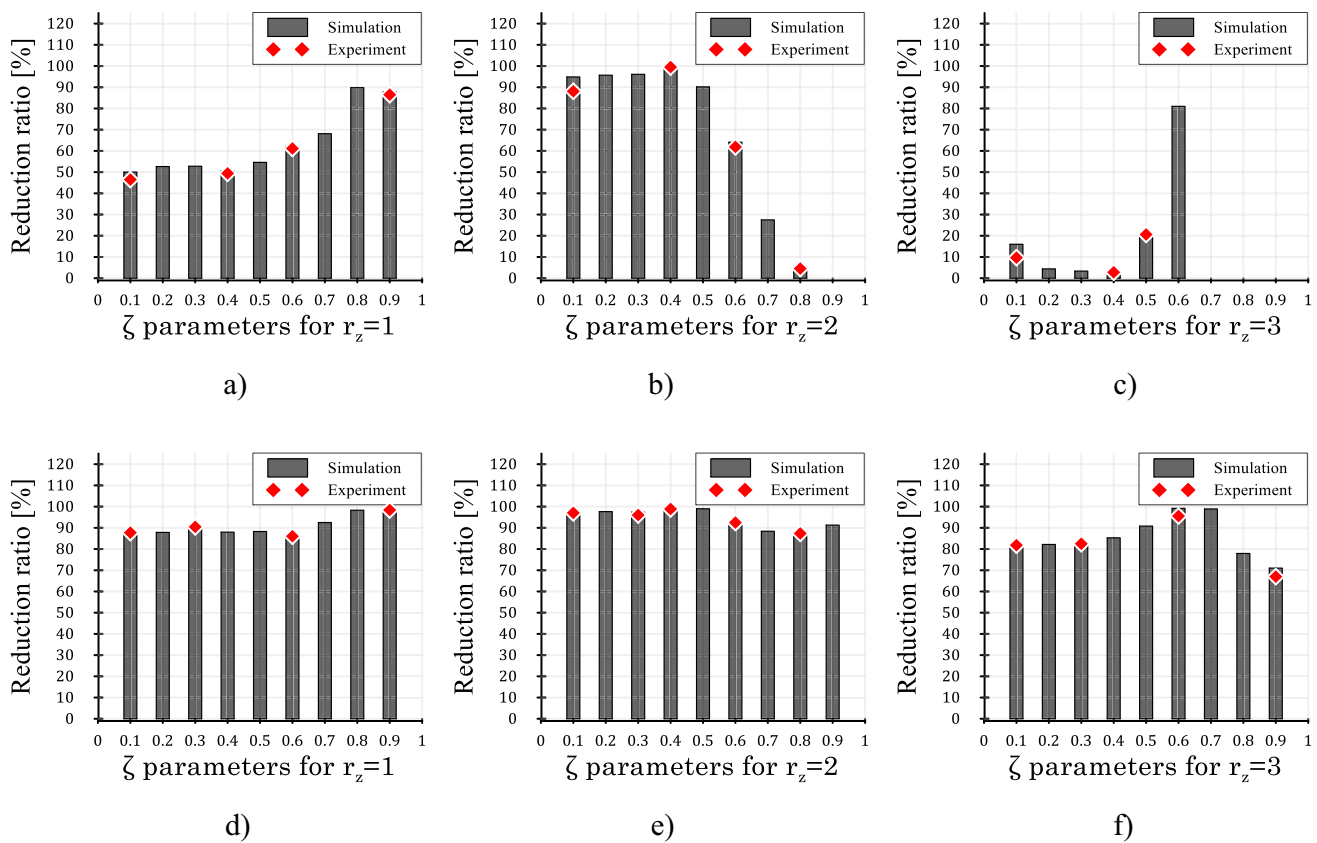


Fig. 15 Reduction ratios according to time parameters of time history acceleration responses for Modification-3, **a–c** $\theta_m = 60^\circ$ and $t_m = 1$ s, **d–f** $\theta_m = 75^\circ$ and $t_m = 1.5$ s

frequencies, regardless of different stopping positions and motion times. While the variation in the maximum and minimum reduction ratios is higher in Modification-3 motion profiles at $\theta_m = 60^\circ$ and $t_m = 1$ s, the change is lower at $\theta_m = 75^\circ$ and $t_m = 1.5$ s. Higher reduction rates are obtained for different time and speed parameter values for $\theta_m = 75^\circ$ compared to $\theta_m = 60^\circ$. However, the maximum reduction ratios obtained for both stopping positions are highly similar.

6 Conclusions

Motion control methods have been used for some time to reduce the endpoint vibrations of robot arms and improve their vibration performance, and studies are ongoing. In the implementation of the method, there are important advantages such as the absence of external influence and the need for an actuator, as well as the disadvantage of being insufficient in terms of completely suppressing residual vibrations when compared to the feedback control method. With motion-based control (MBC), sufficiently reducing the rates of endpoint vibration amplitudes will be very advantageous

in improving the control performance of manipulators where the negative effects of the method will not be taken into account. In this study, an MBC method with three different modified trapezoidal velocity profiles is proposed in order to reduce the endpoint vibrations of single-link composite manipulators of two different lengths.

MBC is accomplished using three newly designed modified velocity profiles. Modified motion profiles are applied both to drive composite manipulators and to reduce endpoint vibrations. The finite element (FE) models of two different composite manipulators for MBC are established in ANSYS, and vibration control is performed by integrating the FE model into the analysis. Three modified motion profiles, namely Modification-1, Modification-2, and Modification-3, are designed based on time and maximum angular velocity parameters using the trapezoidal velocity profile. Using the variation of the parameters of the modified motion profiles, the vibration responses at the tip point of the FCM are obtained. As a result of the analyses performed for all three different motion profiles, the reduction ratios, maximum and minimum vibration amplitudes obtained from the RMS values of the vibration responses of the composite manipulator are obtained. The simulation results are supported by

experimental studies and validated by the modal analysis results and the measured endpoint acceleration vibration responses. Simulation and experimental results have been examined with comparative tables and graphs, and the following conclusions are reached:

- When the results obtained as a result of MBC performed with $\theta_m = 60^\circ$ and $t_m = 1$ s values of motion profiles are compared, the maximum RMS values of the vibration responses at the endpoint of the composite manipulators are found to be 7.8974 m/s², 6.2023 m/s², and 7.7835 m/s² in simulation and 7.6358 m/s², 6.0566 m/s², and 7.4233 m/s² in the experiment for the Modification-1, Modification-2, and Modification-3 motion profiles, respectively, while the minimum RMS values are 0.5386 m/s², 0.2098 m/s², and 0.0352 m/s² in simulation and 0.4980 m/s², 0.1577 m/s², and 0.0373 m/s² in the experiment. With MBC, the endpoint vibration amplitudes are reduced by approximately 14.6, 29.5, and 222.5 times by simulation and 15.2, 39.2, and 200.5 times by the experiment.
- For $\theta_m = 75^\circ$ and $t_m = 1.5$ s motion parameters, the maximum RMS values for the Modification-1, Modification-2, and Modification-3 motion profiles are 6.5721 m/s², 1.4511 m/s², and 1.9046 m/s² in simulation and 6.4179 m/s², 1.4577 m/s², and 2.1183 m/s² in the experiment, respectively, while the minimum RMS values are 0.1614 m/s², 0.1940 m/s², and 0.0544 m/s² in simulation and 0.1716 m/s², 0.2688 m/s², and 0.0725 m/s² in the experiment. The amplitudes with MBC are diminished by about 41.2, 7.6, and 38 times by simulation and 37.7, 5.6, and 30.1 times by the experiment.
- Considering the maximum RMS values of the Modification-1 motion profile as a reference value, for $\theta_m = 60^\circ$ and $t_m = 1$ s motion parameters, maximum reduction ratios for Modification-1, Modification-2 and Modification-3 motion profiles are obtained as 93.18%, 97.34% and 99.55% in simulation studies and 93.48%, 97.93%, and 99.51% in experimental studies, respectively. For $\theta_m = 75^\circ$ and $t_m = 1.5$ s, the reductions are 97.54%, 97.05%, and 99.17% in simulation, and 97.33%, 95.81%, and 98.87%, in experiment, respectively.

When the endpoint vibration responses of FCM are examined, vibration amplitudes with MBC are significantly reduced for all modified motion profiles. It is clear that the Modification-3 motion profile provides better vibration behavior than Modification-1 and Modification-2, although the maximum reduction ratios in MBC are close in all motion profiles in terms of RMS values and decreased ratios of vibration responses. If the endpoint vibrations are desired to be at minimum amplitude in the task plan where the flexible composite manipulator is desired to be performed, it

is recommended to complete the task with Modification-3 motion profiles among the modified motion profiles. Also, in commercial applications, when evaluated in terms of rigid manipulators, MBC will be significantly effective in actuator costs and energy savings by using smaller actuators due to the use of lower-weight manipulators by reducing the endpoint vibration amplitudes in flexible manipulators.

If the reduction ratios and RMS values are considered as design criteria for evaluating the accuracy of the dynamic models of flexible composite manipulators, it is observed that the reduction ratios of the simulation results obtained using FE models match very well with the experiments. The results in all tables and figures reveal that two different composite manipulators with different lengths provide a reduction in the amplitudes of vibration responses in all motion profiles used for MBC for stopping positions and motion times. Experiments indicate that it encourages the implementation of different motion profiles for different manipulators.

Acknowledgements The author expresses his special thanks for the experimental study opportunities provided by Dokuz Eylül University for this study.

Funding The author received no financial support for the research and publication of this article.

Declarations

Conflict of interest The author declares no potential conflicts of interest with respect to the publication of this article.

References

- Abu-Dakka FJ, Assad IF, Alkhdour RM, Abderahim M (2017) Statistical evaluation of an evolutionary algorithm for minimum time trajectory planning problem for industrial robots. *Int J Adv Manuf Technol* 89(1–4):389–406. <https://doi.org/10.1007/s00170-016-9050-1>
- Aikenhead BA, Daniell RG, Davis FM (1983) Canadarm and the space shuttle. *J Vac Sci Technol Vac Surf Films* 1(2):126–132. <https://doi.org/10.1116/1.572085>
- Alandoli EA, Lee TS (2020) A critical review of control techniques for flexible and rigid link manipulators. *Robotica* 38(12):2239–2265. <https://doi.org/10.1017/S0263574720000223>
- Alandoli EA, Sulaiman M, Rashid MZA, Shah HNM, Ismail Z (2016) A review study on flexible link manipulators. *J Telecommun Electron Comput Eng* 8(2):93–97
- ANSYS (2015) Swanson Analysis System
- Benosman M, Le Vey G (2004) Control of flexible manipulators: a survey. *Robotica* 22(5):533–545. <https://doi.org/10.1017/S0263574703005642>
- Boryga M, Graboś A (2009) Planning of manipulator motion trajectory with higher-degree polynomials use. *Mech Mach Theory* 44(7):1400–1419. <https://doi.org/10.1016/j.mechmachtheory.2008.11.003>
- Efafi M, Hosseini SAA, Tourajizadeh H (2022) Robust control and vibration reduction of a 3D nonlinear flexible robotic arm. *Iran*

- J Sci Technol Trans Mech Eng 46(4):1157–1173. <https://doi.org/10.1007/s40997-021-00484-8>
- Esfandiari H, Korayem MH (2015) Accurate nonlinear modeling for flexible manipulators using mixed finite element formulation in order to obtain maximum allowable load. *J Mech Sci Technol* 29(9):3971–3982. <https://doi.org/10.1007/s12206-015-0842-2>
- Fang Y, Qi J, Hu J, Wang W, Peng Y (2020) An approach for jerk-continuous trajectory generation of robotic manipulators with kinematical constraints. *Mech Mach Theory* 153:103957. <https://doi.org/10.1016/j.mechmachtheory.2020.103957>
- Faris WF, AtaSa'adeh AAMY (2009) Energy minimization approach for a two-link flexible manipulator. *J Vib Control* 15(4):497–526. <https://doi.org/10.1177/1077546308095227>
- Gauthier JF, Angeles J, Nokleby S (2006) Optimization of a test trajectory for SCARA systems. *Çinde Advances in Robot Kinematics: Analysis and Design* (ss. 225–234). Springer, Dordrecht. https://doi.org/10.1007/978-1-4020-8600-7_24
- Ghariblu H, Korayem MH (2006) Trajectory optimization of flexible mobile manipulators. *Robotica* 24(3):333–335. <https://doi.org/10.1017/S0263574705002225>
- Kiang CT, Spowage A, Yoong CK (2015) Review of control and sensor system of flexible manipulator. *J Intell Robot Syst Theory Appl* 77(1):187–213. <https://doi.org/10.1007/s10846-014-0071-4>
- Kim SM (2015) Lumped element modeling of a flexible manipulator system. *IEEE/ASME Trans Mechatron* 20(2):967–974. <https://doi.org/10.1109/TMECH.2014.2327070>
- Korayem MH, Irani M, Rafee Nekoo S (2011) Load maximization of flexible joint mechanical manipulator using nonlinear optimal controller. *Acta Astronaut* 69(7–8):458–469. <https://doi.org/10.1016/j.actaastro.2011.05.023>
- Kucuk S (2017) Optimal trajectory generation algorithm for serial and parallel manipulators. *Robot Comput-Integr Manuf* 48:219–232. <https://doi.org/10.1016/j.rcim.2017.04.006>
- Li H, Le MD, Gong ZM, Lin W (2009) Motion profile design to reduce residual vibration of high-speed positioning stages. *IEEE/ASME Trans Mechatron* 14(2):264–269. <https://doi.org/10.1109/TMECH.2008.2012160>
- Liu H, Lai X, Wu W (2013) Time-optimal and jerk-continuous trajectory planning for robot manipulators with kinematic constraints. *Robot Comput-Integr Manuf* 29(2):309–317. <https://doi.org/10.1016/j.rcim.2012.08.002>
- Lochan K, Roy BK, Subudhi B (2016) A review on two-link flexible manipulators. *Annu Rev Control* 42:346–367. <https://doi.org/10.1016/j.arcontrol.2016.09.019>
- Macfarlane S, Croft EA (2003) Jerk-bounded manipulator trajectory planning: design for real-time applications. *IEEE Trans Robot Autom* 19(1):42–52. <https://doi.org/10.1109/TRA.2002.807548>
- MacHmudah A, Parman S, Zainuddin A, Chacko S (2013) Polynomial joint angle arm robot motion planning in complex geometrical obstacles. *Appl Soft Comput J* 13(2):1099–1109. <https://doi.org/10.1016/j.asoc.2012.09.025>
- Malgaca L, İpek Lök Ş, Uyar M (2020) Modeling and vibration reduction of a flexible planar manipulator with experimental system identification. *Int J Model Optim* 10(4):121–125. <https://doi.org/10.7763/ijmo.2020.v10.758>
- Malgaca L, Lök Şİ (2021) Measurement and modeling of a flexible manipulator for vibration control using five-segment S-curve motion. *Trans Inst Meas Control*. <https://doi.org/10.1177/01423312211059012>
- Malgaca L, Uyar M (2019) Hybrid vibration control of a flexible composite box cross-sectional manipulator with piezoelectric actuators. *Compos Part B Eng* 176:107278. <https://doi.org/10.1016/j.compositesb.2019.107278>
- Meggiolaro MA, Dubowsky S, Mavroidis C (2004) Error identification and compensation in large manipulators with application in cancer proton therapy. *Sba Controle & Automação Sociedade Brasileira De Automatic* 15(1):71–77. <https://doi.org/10.1590/S0103-17592004000100009>
- Moghaddam M, Nof SY (2016) Parallelism of Pick-and-Place operations by multi-gripper robotic arms. *Robot Comput-Integr Manuf* 42:135–146. <https://doi.org/10.1016/j.rcim.2016.06.004>
- Nguyen KD, Ng T-C, Chen I-M (2008) On algorithms for planning S-curve motion profiles. *Int J Adv Rob Syst* 5(1):99–106. <https://doi.org/10.5772/5652>
- Pellicciari M, Berselli G, Leali F, Vergnano A (2013) A method for reducing the energy consumption of pick-and-place industrial robots. *Mechatronics* 23(3):326–334. <https://doi.org/10.1016/j.mechatronics.2013.01.013>
- Perumaal S, Jawahar N (2012) Synchronized trigonometric S-curve trajectory for jerk-bounded time-optimal pick and place operation. *Int J Robot Autom* 27(4):385–395. <https://doi.org/10.2316/Journal.206.2012.4.206-3780>
- Preumont A (2018) *Vibration control of active structures: an introduction*. Springer
- Rahimi HN, Nazemizadeh M (2014) Dynamic analysis and intelligent control techniques for flexible manipulators: a review. *Adv Robot* 28(2):63–76. <https://doi.org/10.1080/01691864.2013.839079>
- Rezaei V, Shafei AM (2019) Dynamic analysis of flexible robotic manipulators constructed of functionally graded materials. *Iran J Sci Technol Trans Mech Eng* 43(1):327–342. <https://doi.org/10.1007/s40997-018-0160-2>
- Saravanan R, Ramabalan S (2008) Evolutionary minimum cost trajectory planning for industrial robots. *J Intell Robot Syst Theory Appl* 52(1):45–77. <https://doi.org/10.1007/s10846-008-9202-0>
- Sayahkarajy M, Mohamed Z, Mohd Faudzi AA (2016) Review of modelling and control of flexible-link manipulators. *Proc Inst Mech Eng Part I J Syst Control Eng* 230(8):861–873. <https://doi.org/10.1177/0959651816642099>
- Shitole C, Sumathi P (2015) Sliding DFT-based vibration mode estimator for single-link flexible manipulator. *IEEE/ASME Trans Mechatron* 20(6):3249–3256. <https://doi.org/10.1109/TMECH.2015.2391132>
- Tinkir M, Önen Ü, Kalyoncu M (2010) Modelling of neurofuzzy control of a flexible link. *Proc Inst Mech Eng Part I J Syst Control Eng* 224(5):529–543. <https://doi.org/10.1243/09596518JSC785>
- Uyar M (2022) Comparison of classical and newly designed motion profiles for motion-based control of flexible composite manipulator. *J Braz Soc Mech Sci Eng* 44(9):414. <https://doi.org/10.1007/s40430-022-03725-2>
- Wang B, Lou J (2019) Coupling dynamic modelling and parameter identification of a flexible manipulator system with harmonic drive. *Meas Control (United Kingdom)* 52(1–2):122–130. <https://doi.org/10.1177/0020294018823026>
- Wu H, Sun D (2019) High precision control in PTP trajectory planning for nonlinear systems using on high-degree polynomial and cuckoo search. *Opt Control Appl Methods* 40(1):43–54. <https://doi.org/10.1002/oca.2464>

Springer Nature or its licensor (e.g. a society or other partner) holds exclusive rights to this article under a publishing agreement with the author(s) or other rightsholder(s); author self-archiving of the accepted manuscript version of this article is solely governed by the terms of such publishing agreement and applicable law.